Numerical simulation of interactions between dissociating gases and catalytic materials in shock tubes

V.V. Riabov

Department of Computer Science, Rivier College, Nashua, New Hampshire 03060 USA

Summary. A numerical method has been developed to study interactions between gas flows and catalytic materials of the shock-tube end after shock wave reflection at high temperature conditions. The study is based on computations of nonequilibrium multicomponent gasdynamic parameters in air and analysis of the nonsteady-state thermal boundary layer near the tube end.

1 Introduction

Shock tubes have become widely used to study thermodynamic processes in high temperature gas flows [1], [2] and chemical kinetics [3], [4]. Flow parameters behind incident and reflected shock waves were analyzed by Gaydon and Hurle [1], Bazhenova et al. [2], Sturtevant and Slachmuylders [5], Goldsworthy [6], Johannesen et al. [7], and Hanson et al. [8]. It was found that the gas behind the reflected shock wave is practically at rest in the laboratory coordinate system, and the temperature in this area is approximately twice as high as behind the incident shock wave.

The purpose of the present study is to analyze heat transfer processes at the catalytic materials of the shock-tube end after shock wave refraction in terms of the model of the nonsteady-state nonequilibrium thermal boundary layer developed by Provotorov and Riabov [9], [10], [11]. The analysis [9] covered the time interval from 10^{-9} sec to 2.5 μsec, and it was restricted by the applied numerical method. In the present study we have developed the numerical algorithm and studied gasdynamic parameters and component concentrations in the layer for the time interval up to 100 μsec. The parameters behind the reflected shock wave [1], [2], [9], [11] were evaluated as the external boundary conditions for the layer. The nonequilibrium parameters in this area are the functions of initial parameters such as pressure and temperature in the shock-tube channel, velocity of the incident shock wave, etc. The dissociation, recombination and exchange reactions [4], [12] among the air components (O_2, O, NO, N_2, and N) were considered. At the shock-tube end a union boundary condition [5], [6], [7], [9] for temperature and heat flux was used, as well as a boundary condition for recombination of atomic components. Unfortunately, the identical experimental data are unknown to the author.

2 Gas flow behind the incident shock wave

We have considered the simplest model [1], [2], [9] of the one-dimensional inviscid dissociating gas flow behind the incident shock wave, which propagated in an ideal air with parameters of pressure $p_1 = 1$ and 100 Pa, and temperature $T_1 = 295$ K at constant velocity $U_S = 5$ km/s. The system of chemical reactions occurring in the five-component mixture and reaction constants used in the present study were described in [4], [12].

The algorithm of calculation of the parameters behind the incident and reflected shock waves is described by Provotorov and Riabov [9] in detail. The system of algebraic-differential equations [9] has been solved at each point of the flow field behind the incident shock wave under the assumption that air is not dissociated on the shock wave front. A modified Newton's method [13] with optimal choice of iteration step was used for numerical solution of the equations. The flow parameters behind the incident shock wave

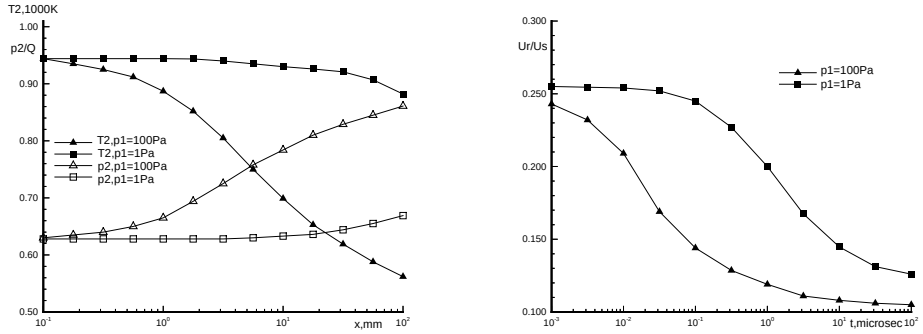

Fig. 1. Temperature T_2 and pressure p_2 behind the incident shock wave as a function of distance from the wave front (*left*), and velocity of the reflected shock wave U_{R} as a function of time (*right*) at various initial pressure parameters: $p_1 = 1$ Pa (*squares*) and $p_1 = 100$ Pa (*triangles*)

are shown in Fig. 1 (*left*). The solutions obtained for temperature and pressure are typical for dissociating gas flows with nonequilibrium relaxation [1], [2], [7], [8], [9]. For small time interval ($t \approx 10^{-8}$ sec) the gas state is frozen [2], while at large distances from the shock wave (at $t \geq 10^{-5}$ sec and $p_1 = 100$ Pa) the flow parameters tend to their limiting equilibrium values [2]. With decrease in initial pressure up to $p_1 = 1$ Pa the equilibrium state is reached at significantly distances, while at $t < 10^{-5}$ sec the flow parameters differ little from frozen.

3 Gas flow behind the reflected shock wave

The reflected shock wave is propagated in the disturbed field after the incident shock wave [7], [8]. The velocity of the reflected shock wave U_{R} as a function of time, for two cases of pressure $p_1 = 1$ and 100 Pa, is plotted in Fig. 1 (*right*) (squares and triangles, correspondingly). The decrease of the values U_{R} indicates the nonequilibrium type of chemical reactions behind the incident shock wave [8]. The magnitude of pressure p_1 defines the time required for attainment of the steady-state distribution. And this time is less by approximately a factor of 100 for the case of $p_1 = 100$ Pa. Therefore, the parameter U_{R} becomes very convenient for experimental verification of the nonequilibrium parameters in the areas behind the shock and near the end of the tube.

Using the technique developed by Provotorov and Riabov [9], the distribution of temperature T_3 and pressure p_3 behind the reflected shock wave was calculated. The computational technique was used as the same one that was discussed above for the case

of the incident shock wave. The computational results are shown in Fig. 2 (*left*) at the same cases of the initial pressure p_1. The distribution of temperature T_3 [see Fig. 2 (*left*)] is similar to the distribution of the velocity U_{R} of the reflected shock wave and it can be useful for the identification of the type of the chemical processes behind the shocks [7], [8]. The values of temperature $T_3(\mathrm{t})$ were used as the external ("outer") boundary conditions for temperature in the thermal viscous layer near the tube end. Figure 2 (*left*) presents

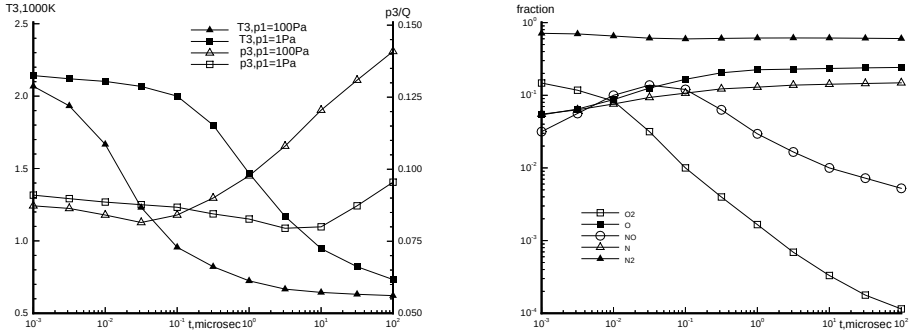

Fig. 2. Temperature T_3 and pressure p_3 behind the reflected shock wave as a function of time at various initial pressure parameters: $p_1 = 1$ Pa (*squares*) and $p_1 = 100$ Pa (*triangles*) (*left*), and mass fractions α_{i} in air behind the reflected shock wave at $p_1 = 100$ Pa (*right*)

also the computational results for pressure p_3 behind the reflected shock wave as a function of time. This parameter is the most conservative one. Nevertheless, for the case of the large value of initial pressure $p_1 = 100$ Pa (triangles) the significant increase of the values p_3 is observed after the short initial time-interval of decreasing. This is a result of the influence of different types of chemical relaxation processes behind the incident wave with initial pressure p_1 [5], [6], [8], [9]. The initial decrease of p_3 is explained by rapid chemical relaxation behind the reflected shock wave [8]. As presented in Fig. 2 (*left*), the temperature distribution $T_3(\mathrm{t})$ indicates this type of chemical process in the region. In the case $p_1 = 100$ Pa, the flow behind the reflected shock wave is close to a state of local thermodynamic equilibrium [2], while in the other case $p_1 = 1$ Pa, the flow is significantly in nonequilibrium [8], [9]. The function $p_3(\mathrm{t})$ can be used for the prediction of pressure in the thermal viscous layer near the tube end, and it correlates with the value of pressure $p_{\mathrm{w}}(\mathrm{t})$ at the tube end.

Additional important information is the distribution of the air components behind the reflected shock wave. This data [shown in Fig. 2 (*right*)] has been used as external boundary conditions for the component mass concentrations in the thermal viscous layer under the considered conditions.

4 The thermal viscous layer near the tube end

Behind the reflected shock wave the thermal viscous layer begins to grow near the tube end [5], [6], where a union boundary condition for temperature and heat flux is used,

as well as a boundary condition for recombination of atomic components. The acceptable model of a nonsteady-state nonequilibrium thermal boundary layer [6], [9] could be considered in this area. The gasdynamic functions in the layer are determined by the following dimensional parameters [9]: t_*, ρ_*, μ_*, $p_* = \rho_* {U_S}^2/2$, $l = U_S t_*$, $\delta_* = (\mu_* t_*/\rho_*)^{0.5}$, $u_* = \delta_*/t_*$, which are the characteristic time, density, viscosity, pressure, length, and layer thickness. Below we treat all functions and variables as dimensionless, referenced to their characteristic values.

Comparing the values of two parameters l and δ_*, the main perturbation parameter ϵ can be introduced:

$$\epsilon^2 = (\delta_*/l)^2 = \mu_*/(\rho_* {U_S}^2 t_*)$$

Using the perturbation technique, the independent variables and functions in the near-wall flow area at the tube end can be described in terms of series [9], [10]:

$$x = \epsilon x^{(1)} + ..., t = t^{(0)}, u = \epsilon u^{(1)} + ..., T = T^{(0)} + ..., \rho = \rho^{(0)} + ..., \alpha_i = {\alpha_i}^{(0)} + ...$$

If we substitute transformation (3) in a system of nonsteady-state one-dimensional Navier-Stokes equations and transform to the limit $\epsilon \to 0$, we obtain the system of equations of the thermal nonequilibrium boundary layer that was analyzed by Provotorov and Riabov [9], [10] in detail. Air is considered as a multicomponent system of five components (O_2, O, NO, N_2, and N). The mass diffusion flux, viscosity, and heat conductivity of multicomponent gas mixture were calculated by the approximation method of Riabov [17]. To satisfy the continuity equation identically, the stream function ψ was introduced, as well as new independent variables:

$${\psi'}_t = -\rho u;\ {\psi'}_x = \rho;\ \tau = t;\ \eta = \psi/(2t)^{0.5}$$

After transformations we obtain a system of partial differential equations of the parabolic type. A finite-difference approximation to the boundary-layer equations, with boundary conditions mentioned above, was constructed analogous to the method using a matrix variant of Keller's two-point "box scheme" [14], [15], [16]. The spatial and time variables were approximated by the second order terms. The finite-difference stability analysis has been performed by Denisenko and Provotorov [14] in terms of the spectral method. The two-point difference equations were solved by the matrix regularization technique of Provotorov [15].

5 Heat flux at the catalytic wall

The calculated values of heat transfer coefficient $C_h = q/(\rho_1 {U_S}^3)$ are shown in Fig. 3 (*left*) for the range of time t = 10^{-8} – 10^{-4} sec and initial pressure p_1 = 1 and 100 Pa (triangles and squares, correspondingly). At t < 1 μsec the heat flux values differ by a factor of 50. At t > 10 μsec this difference is less significant. The thermal layer state approaches equilibrium at p_1 = 100 Pa, and the heat flux values are almost the same for various catalytic materials (see Fig. 3 (*left*); filled triangles for Pyrex, empty triangles for nickel). At lower initial pressure p_1 = 1 Pa, processes within the thermal layer are of a strongly nonequilibrium character. For this case, the influence of catalytic properties

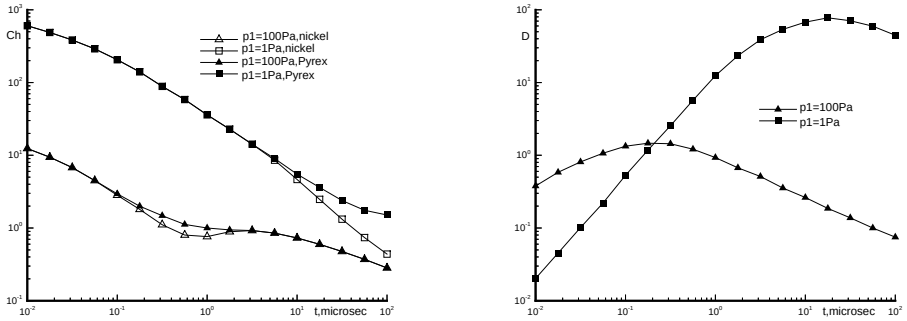

Fig. 3. Heat transfer coefficient $C_{\rm h}$ (*left*) and normalized thermal boundary layer thickness D $= 10^5\delta/(U_{\rm S}t_*)$ (*right*) at the end wall of the shock tube for various wall catalytic properties and initial pressure parameters: $p_1 = 1$ Pa (*squares*) and $p_1 = 100$ Pa (*triangles*)

of the wall material is significant. For different catalytic materials [see Fig. 3 (*left*); filled squares for Pyrex, empty squares for nickel] the values of heat transfer coefficient $C_{\rm h}$ differ by a factor of 6 at t > 30 μsec. This phenomenon can be applied to the identification of catalytic properties of heat protection materials.

6 The chocking effect in the thermal viscous layer

Figure 3 (*left*) shows the anomalous behavior of the $C_{\rm h}$(t) function for large times (t $>$ 0.4 μsec) at $p_1 = 100$ Pa. It indicates on the "chocking" effect in the thermal boundary layer. The time development of thermal layer thickness D $= 10^5\delta/(U_{\rm S}t_*)$ is shown in Fig. 3 (*right*). The thermal boundary layer thickness is defined as

$$\delta = (2\tau)^{0.5} \int_0^{\eta_\delta} \rho^{-1}{\rm d}\eta.$$

Here parameter η_δ is the η value at the external boundary of the thermal layer. Parameter t_* is equal to 100 μsec.

In the case $p_1 = 100$ Pa there exist well-defined moments in time at which the layer thickness (triangles) reaches a maximum value. Pressure behind the reflected shock wave p_3(t) begins to grow at these moments [see Fig. 2 (*left*), triangles]. This flow regime is characterized by the value $p_1 = 100$ Pa. The similar effect is also identified for larger times (t > 20 μsec) at lower initial pressure $p_1 = 1$ Pa [see squares in Fig. 3 (*right*)]. Such a mechanism is possible only in nonequilibrium gas, where physical and chemical processes allow maintaining a positive pressure gradient dp/dt [8], [9]. The chocking is caused by decreasing the layer thickness δ, when the pressure p_3(t) is increasing.

7 Conclusion

A method based on the numerical analysis of the thermal boundary layer near the shock tube end has been developed for studying heat transfer properties of catalytic materials

at high temperatures. The dependence of heat flux and pressure at the shock tube end as well as reflected shock wave velocity upon time provides valuable information on the characteristics of the thermal boundary layer near the tube end and catalytic-wall properties. The same flow characteristics can be used for determination of the discovered chocking effect of the nonsteady-state nonequilibrium thermal boundary layer near the tube end.

The analysis was made in terms of one-dimensional nonsteady flow models. In future studies the possible effects of the boundary layers on the tube sidewall should be taken into consideration. However, the problem of an interaction between the sidewall boundary layers with the thermal boundary layer at the shock tube end wall would require a three-dimensional analysis for a correct interpretation of future experimental results.

Acknowledgement. The author expresses gratitude to V. P. Provotorov for participation in developing numerical algorithms.

References

1. A.G. Gaydon, I.R. Hurle: *The Shock Tube in High-Temperature Chemical Physics* (Reinhold, New York 1963)
2. T.V. Bazhenova, L.G. Gvozdeva, Yu.G. Lobastov: *Shock Waves in Real Gases* (Nauka, Moscow 1968)
3. M.W. Slack: J. Chem. Phys. **64**, 228 (1976)
4. C. Park, J.T. Howe, R.L. Jaffe, G. Candler: J. Thermophys. Heat Transf. **8**, 9 (1994)
5. B. Sturtevant, E. Slachmuylders: Phys. Fluids **7**, 1201 (1964)
6. F.A. Goldsworthy: J. Fluid Mech. **5**, 164 (1959)
7. N.H. Johannesen, G.A. Bird, H.K. Zienkiewicz: J. Fluid Mech. **30**, 51 (1967)
8. R.K. Hanson, L.L. Presley, E.V.Williams: Numerical solutions of several reflected shock-wave flow fields with nonequilibrium chemical reactions. NASA TN D-6585 (1972)
9. V.P. Provotorov, V.V. Riabov: J. Appl. Mech. Techn. Phys. **28**, 721 (1987)
10. V.V. Riabov, V.P. Provotorov: AIAA Paper 2071 (1994)
11. V.V. Riabov, V.P. Provotorov: J. Thermophys. Heat Transf. **9**, 363 (1995)
12. V.P. Provotorov, V.V. Riabov: Tr. TsAGI **2111**, 142 (1981)
13. V.V. Ermakov, N.I. Kalitkin: J. Comput. Math. Math. Phys. **21**, 235 (1983)
14. O.V. Denisenko, V.P. Provotorov: Tr. TsAGI **2269**, 1 (1985)
15. V.P. Provotorov: Tr. TsAGI **2436**, 165 (1990)
16. V.V. Riabov: Three fast computational approximation methods in hypersonic aerothermodynamics. In: *Computational Fluid and Solid Mechanics*, ed. by K. J. Bathe (Elsevier: Boston 2005), 819–823
17. V.V. Riabov: J. Thermophys. Heat Transf. **10**, 209 (1996)